Journal of Solid State Chemistry **149,** 298–307 (2000)
doi:10.1006/jssc.1999.8530, available online at http://www.idealibrary.com on IDEAL®

# A High-Pressure Raman Study of Mixed Perovskites $BaCe_xZr_{1-x}O_3$ $(0 \leq x \leq 1)$

C. Chemarin, N. Rosman, T. Pagnier, and G. Lucazeau[1]

*Laboratoire d'Electrochimie et de Physicochimie des Matériaux et des Interfaces, ENSEEG-INPG, B.P. 75, 1130 rue de la piscine, 38 402 St. Martin d'Héres Cedex, France*
E-mail: lucazeau@inpg.fr

Received August 3, 1999; in revised form September 30, 1999; accepted October 11, 1999

**A high-pressure Raman study of polycrystalline samples of $BaCe_xZr_{1-x}O_3$ is performed at room temperature. The evolution of Raman spectra with pressure is compared to the evolution of the Raman spectra of $BaZrO_3$ and $BaCeO_3$. The effect of composition on the pressure-induced phase transitions is monitored from the Raman spectra. Transitions toward lower symmetry phases as pressure increases are evidenced. A phase diagram in the binary system $BaZrO_3$–$BaCeO_3$ based on the Raman spectra characteristic of the different structures of $BaCeO_3$ (*Pnma*, *Imma*, $R\bar{3}c$, *Pm3m*) is proposed. The transition pressures toward low-symmetry structures decrease when Ce is replaced for Zr. This study allows us to interpret the $BaCe_xZr_{1-x}O_3$ $(0 \leq x \leq 1)$ Raman spectra at ambient pressure on the basis of nanodomains and nanophases. These objects tend to disappear upon pressure increase. The octahedra to dodecahedra volumes ratio is used as a critical parameter that is able to reproduce qualitatively some of the phase transitions in the mixed perovskites $BaCe_xZr_{1-x}O_3$. In order to calculate this parameter vs pressure, a derivation of the samples' compressibility based on a polyhedral approach is performed and is found in the range $[0.7\times10^{-11}$–$1.0\times10^{-11}$ $Pa^{-1}]$.** © 2000 Academic Press

***Key Words*: perovskite; Raman spectroscopy; high pressure; phase diagram; compressibility.**

## 1. INTRODUCTION

Substitution-induced structural disorder in mixed ionic crystals is still not completely understood. For a crystal in which an atom B can be substituted for an A atom of the same (formal) valence and charge, the distribution of A and B on the A sites can sometimes be described as fully random with properties ranging between those of the extreme compositions (model I) or in terms of nanophases for which the properties are those of composite materials (model II) (1). These two models have been used in the literature for interpreting experimental results depending upon the correlation length of the characterization technique used. Some solid solutions of perovskites are considered to be made of coexisting nanophases which are impossible to identify by conventional diffraction techniques but which can be guessed from TEM (2, 3) or by short-range techniques such as Raman spectroscopy (4). The spectroscopic data of solid solutions (see (5) for a review) give rise to the so-called one- and two-mode behaviors of eigenfrequencies. In the one-mode behavior, the frequency varies continuously from one end member to the other (e.g., $Sr_xBa_{1-x}F_2$ (6). In this case, it is possible to interpret the results with the use of an "average-ion" the properties (mass, force constant) of which lie between those of *A* and *B*. In contrast, two frequencies can be identified in the two-mode behavior ($Si_{1-x}Ge_x$ (7)) and *A* and *B* atoms keep their individuality. Both kinds of behaviors can be found in the same material, as is the case in $BaCe_xZr_{1-x}O_3$ (8). In this system, the problem of substitution-induced structural disorder is not yet solved. The application of pressure is expected to help in the identification of possible nanophases which would have a behavior toward pressure quite different from that of a statistically long-range ordered system. Hence, for model I, pressure could induce structural changes at long range and lead to changes of space group. For model II, the pressure effect could induce changes at short range and help to discriminate between two nanophase types, providing they do not interact too strongly.

In other respects, doped $ABX_3$ perovskite structures have been of special interest as ceramic protonic conductors. Rare-earth-doped $BaCeO_3$ exhibits good proton conduction in atmospheres containing hydrogen and/or water vapor at elevated temperatures (9). However, this compound is not stable enough from chemical and mechanical points of view for electrochemical applications (10). In this respect $BaZrO_3$ has been found to be chemically more stable and to have better mechanical properties than $BaCeO_3$. Nevertheless proton conduction in doped zirconates is lower (10).

[1]To whom correspondence should be addressed.



0022-4596/00 $35.00

Hence, the study of the effects of Zr substitution for Ce in these materials on their conductivity (11) and their mechanical properties can be useful for future fuel cell applications.

A first study of Raman spectra and XRD patterns of $BaCe_xZr_{1-x}O_3$ (8) as a function of composition and temperature allowed us to conclude that $BaCeO_3$ and $BaZrO_3$ were miscible in all proportions and to propose a phase diagram based on the low-wavenumber Raman bands. Starting from $BaCeO_3$ at room temperature, phase transitions occurred in the order *Pnma–Imma–R*$\bar{3}$*c–Pm3m* either by heating or by replacing Ce by Zr. For the intermediate compositions, the order in which transitions appeared remained the same, starting at room temperature from *Imma* for $x = 0.8$ and $x = 0.6$, *R*$\bar{3}$*c* for $x = 0.4$ and $x = 0.2$, or from *Pm3m* for $x = 0.1$ and $x = 0$. These attributions were based on the number of bands at low frequencies (80–150 $cm^{-1}$), three for *Pnma*, two for *Imma*, one for *R*$\bar{3}$*c*, and no bands for *Pm3m*; for this last space group, no Raman transition is allowed (Fig. 1). These space group determinations, based on the symmetry properties of Raman transitions and on correlations with the well-known temperature phase transition of $BaCeO_3$ (12, 13), were later confirmed by neutron diffraction (14). One of the interesting results of this previous study was the observation of a Raman spectrum for $BaZrO_3$ (theoretically forbidden by symmetry), which was interpreted as mainly made of first-order bands and of some second-order Raman bands. Later measurements of Raman spectra under pressure (11) led to the conclusion that the origin of the first Raman spectra was most probably induced by a dynamical disorder in the material. The first objective is to study the behavior of the solid solutions under pressure, with the hope that this can provide information about the structure of pure $BaZrO_3$ at ambient pressure. For this purpose the $BaZrO_3$ spectra taken by Cougoulic (11) are revisited. A second objective of this paper is to study the $BaCe_xZr_{1-x}O_3$ phase transitions as a function of pressure and to sketch a qualitative ($x$, $P$) diagram.

In the first part of the Discussion, we report on the $BaCeO_3$–$BaZrO_3$ phase diagram which is based on Raman spectra changes. In the second part, we try to derive compressibilities from the evolution of Raman frequencies with applied pressure in order to predict structural changes and to reproduce the phase transitions. Using the concept of polyhedra compressibility originally proposed by Hazen (15), compressibilities are derived from the method described in (16) and based on the Grüneisen model. After recalling the different definitions and equations used, we justify our choice of localized modes from which the individual polyhedra compressibilities are calculated. This procedure is based on previous vibrational normal mode calculations performed on $BaCeO_3$ (17) which can help us identify stretching modes involving one kind of polyhedra. Finally the ($x$, $P$) phase diagram is presented.

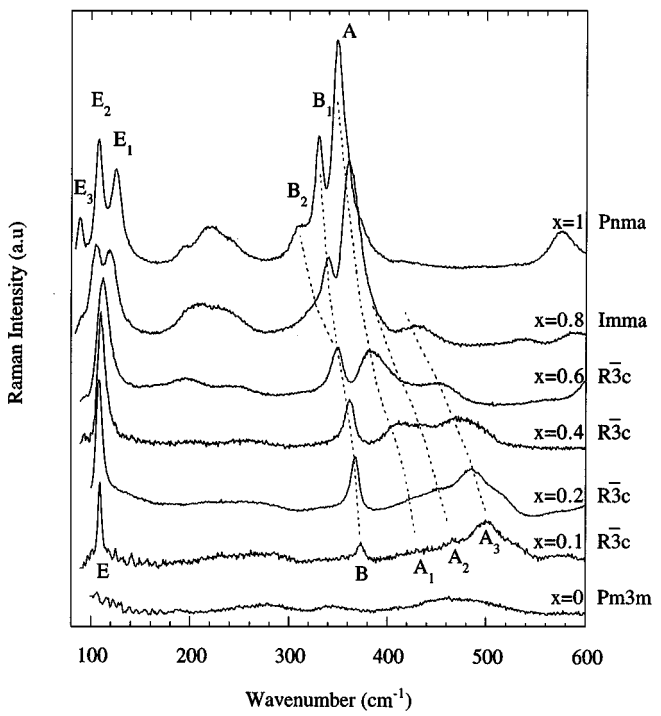


**FIG 1.** Raman spectra of $BaCe_xZr_{1-x}O_3$ samples at ambient pressure and temperature. The $x$ values are indicated at the right of each spectrum. Band labels ($A_i$, $B_i$, $E_i$) are reported.

## 2. EXPERIMENTAL

### 2.1. Sample Preparation

$BaCe_xZr_{(1-x)}O_3$ samples were prepared by solid-state reaction. High purity powders of $BaCO_3$ (Rhône-Poulenc), $CeO_2$ (Rhône-Poulenc), and $ZrO_2$ (Tosoh) in stoichiometric amounts were mixed for 15 h. The mixture was first calcined in air at 950°C for 15 h in order to prevent an irreversible expansion during sintering due to $BaCeO_3$ decarbonatation. The powders were then ground in an agate mortar and pressed into pellets at an uniaxial pressure of 50 MPa followed by isostatic pressure at 250 MPa. Sintering was performed in air at 1500°C for 10 h, and samples were furnace cooled at about 2°C · $min^{-1}$. The presence of well-developed crystallites of either end member has not been detected in diffraction experiments (8, 14) (a linear relationship between the cell parameters and $x$ is observed). Furthermore $BaCeO_3$ in its *Pnma* form has a strong first-order Raman spectrum, and its presence should have been observed in the Raman spectra of the mixed compounds even for very small crystallites of the order of 10 nm. Figure 1 shows that the *Pnma* $BaCeO_3$ spectrum does not appear on $BaCe_xZr_{(1-x)}O_3$ ($0 \le x < 1$) spectra. These observations indicate a strong mixing effect and therefore mutual solubility.

From an elemental analysis on all the samples, a systematic deficit of about 1% of Zr is found.

### 2.2. Raman Spectroscopy

Raman spectra were recorded at room temperature with an XY Dilor multichannel spectrometer under a microscope in backscattering geometry. Radiation of 514.53 nm from an argon ion laser with an incident power of 20 mW through a $\times 20$ objective of a microscope was used; the analyzed area was about 2 $\mu m^2$.

### 2.3. High-Pressure Experiments

A high-pressure diamond anvil cell was used. Samples were set in a chamber 250 μm in diameter and 50 μm thick, and the samples dimensions were about $30 \times 50 \times 50$ $\mu m^3$. The pressure in the cell was monitored by the wavenumber shift of the $^2F_g \rightarrow {}^4A_{2g}$ fluorescence bands of $Cr^{3+}$ ions of a small ruby crystal placed in the vicinity of the sample (18). The pressure-transmitting fluid was a 4:1 methanol–ethanol mixture. The studies were performed from ambient pressure up to 33 GPa with a step of about 3 GPa for each compound. The spectra were systematically decomposed into individual Lorentzian components with Jandel Peakfit Software.

The pressure isotropy can be checked from the ruby fluorescence spectrum. Its two well-resolved Lorentzian-shaped components indicate an hydrostatic pressure up to ca. 10 GPa (vitrification pressure of the methanol–ethanol mixture (18)). For higher pressures, a band broadening appears. This is characteristic of a distribution of pressures in the chamber. From the full width at half maximum of the bands, it can be estimated to 13–17 GPa at a mean pressure of 15 GPa and 27–33 GPa at 30 GPa.

## 3. RESULTS

Room-temperature and room-pressure spectra are shown in Fig. 1. As compared to previous results (8, 11), the $BaCe_{0.1}Zr_{0.9}O_3$ spectrum contains two narrow bands which indicate that the structure is $R\bar{3}c$ instead of *Pm3m*. In the same way, the $BaCe_{0.6}Zr_{0.4}O_3$ spectrum is closer to that of the $R\bar{3}c$ structure instead of the *Imma* structure. These two compositions are very close to the boundary compositions of $Pm3m$–$R\bar{3}c$ and $R\bar{3}c$–*Imma* transitions, and small changes in composition can affect the structure. One may distinguish between three groups of bands with different behaviors: (i) below 150 $cm^{-1}$, three bands labeled $E_i$ ($i = 1$, 2, 3) in $BaCeO_3$ merge to a single band E for $x = 0.1$; (ii) near 300 $cm^{-1}$, two bands $B_1$ and $B_2$ are present in $BaCeO_3$ spectra and merge in a single band B for $x = 0.1$; (iii) an intensity transfer occurs between the $A_i$ ($i = 1, 2, 3$) bands. $A_1$ intensity increases with $x$ to the detriment of $A_3$ intensity. These bands exhibit a strong frequency dependence with composition.

Figures 2–5 present the pressure effect on the Raman spectra of some compositions. For $BaZrO_3$ (Fig. 2) a clear spectral change is observed above 9 GPa and can be associated with a phase transition. Notice also that most of the broad bands observed at 1 atm tend to disappear when $P$ increases up to 9 GPa. In the same way a second change is observed above 23 GPa, characterized by the B band splitting. A continuous wavenumber increase is observed from 12 to 30 GPa, indicating a regular behavior (no anharmonic couplings, no soft modes). Figure 3 represents the $BaCe_{0.1}Zr_{0.9}O_3$ Raman spectra up to 35 GPa. The $A_3$, B, and E band wavenumbers increase continuously when pressure increases. At about 15 GPa, B and E bands exhibit a splitting which can be associated with a phase transition. Figure 4 presents the pressure effect on the $BaCe_{0.8}Zr_{0.2}O_3$ Raman spectra. The band wavenumbers increase continuously with pressure up to 27 GPa. Above this pressure the broad bands appearance at about 500 and 750 $cm^{-1}$ indicate a phase transition. Figure 5 shows the B band splitting for $0 \leq x \leq 1$. The splitting pressure increases with decreasing $x$. Notice that the band widths of $BaCe_xZr_{1-x}O_3$ for

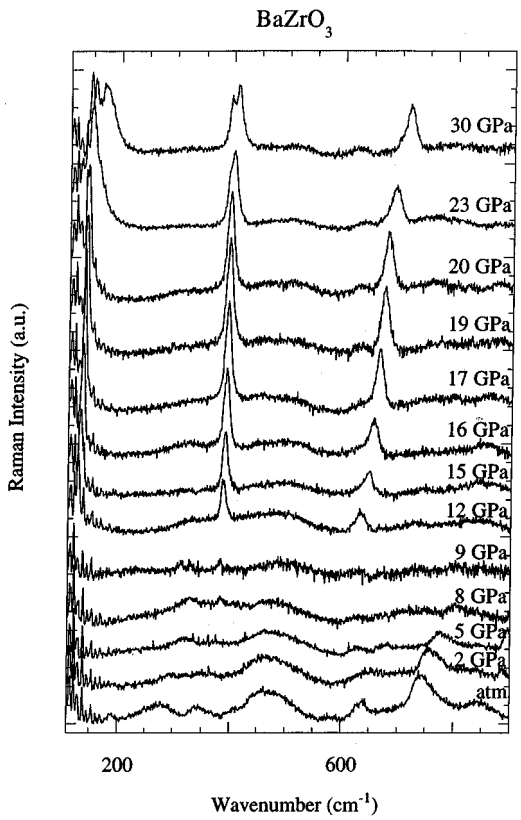


**FIG. 2.** Raman spectra of $BaZrO_3$ between 0 and 30 GPa (7). The spectra have been baseline corrected.

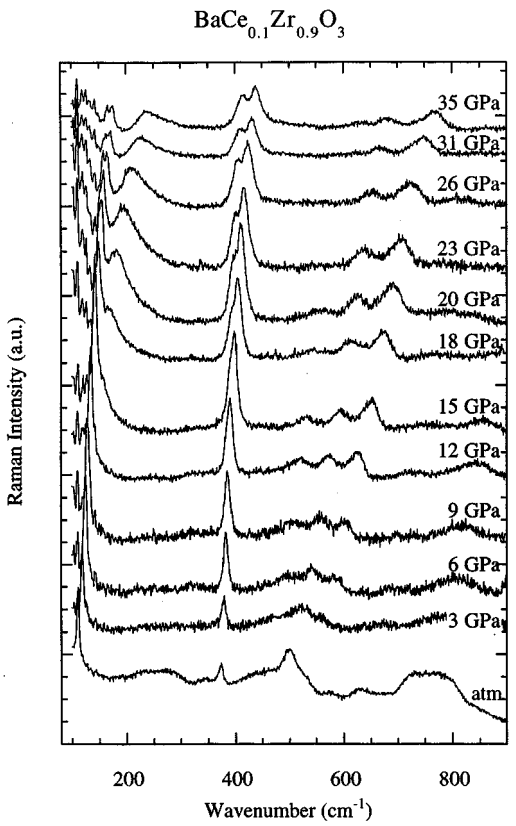


**FIG. 3.** Raman spectra of $BaCe_{0.1}Zr_{0.9}O_3$ between 0 and 35 GPa. The spectra have been baseline corrected.

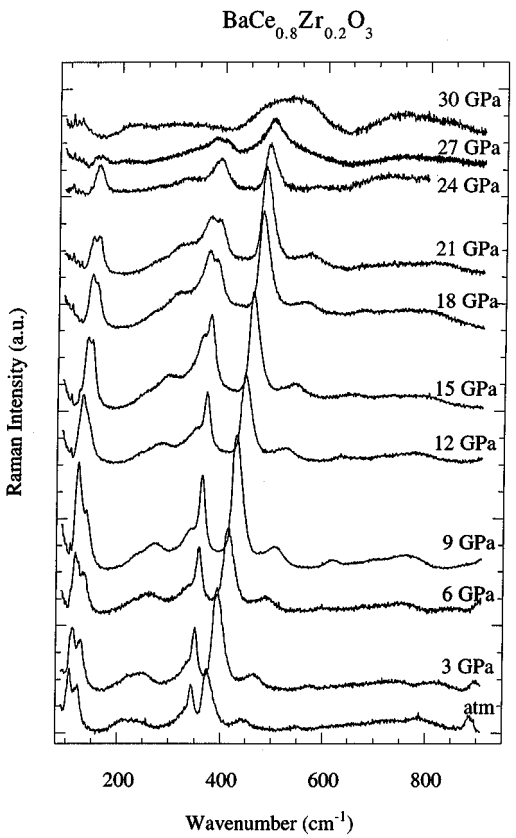


**FIG. 4.** Raman spectra of $BaCe_{0.8}Zr_{0.2}O_3$ between 0 and 30 GPa. The spectra have been baseline corrected.

$0 < x < 1$ are more important than the $BaZrO_3$ ones at high pressure. Figure 6 compares the high-pressure spectra of $BaCeO_3$, $BaCe_{0.8}Zr_{0.2}O_3$, and $BaCe_{0.6}Zr_{0.4}O_3$. Notice for $x = 1$, $x = 0.8$, and $x = 0.6$ the presence of a broad band near 550 $cm^{-1}$. Another broad band appears for $x = 0.8$ at about 750 $cm^{-1}$ and increases in intensity and wavenumber with increasing Zr content. Finally Fig. 7 compares the pressure effect on the $x = 0.1$ and $x = 0.2$ compositions. For $x = 0.1$, the B band intensity is lower than that of the $A_i$ bands at 1 atm while its intensity is higher for $x = 0.2$. At high pressure the B band intensity is much higher than the $A_i$ ones for the two compositions.

## 4. DISCUSSION

### *4.1. Phase Transitions of $BaCe_xZr_{(1-x)}O_3$ with Pressure*

An assignment of Raman-actives modes of $BaCeO_3$ was performed from a normal modes calculation (17), and it is thus possible to identify modes which involve stretching coordinates in octahedra or dodecahedra of the *Pnma* structure. $E_i$ bands (Fig. 1) below 150 $cm^{-1}$ are mostly due to Ba–O stretching and O–Ba–O bending force constants. $B_i$ bands involve Ba–O stretching and O–Ce–O bending. The A band is almost exclusively correlated to the Ce–O stretching force constant. This band assignment is likely still valid in the mixed compounds (8): the intensity exchange

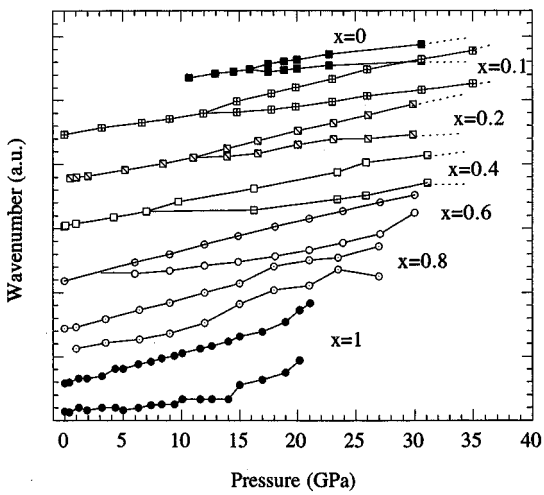


**FIG. 5.** The $\omega = f(P)$ plots for the B Raman band of the perovskite structure. The splitting of the B band corresponds to the transition $R\bar{3}c \rightarrow Imma$.

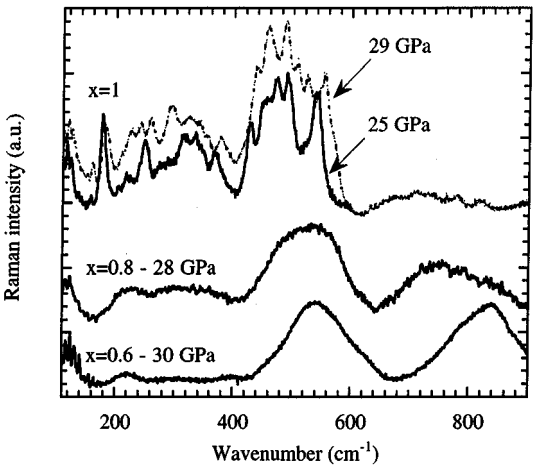


**FIG. 6.** Raman spectra of $BaCeO_3$ at 25 and 29 GPa, $BaCe_{0.8}Zr_{0.2}O_3$ at 28 GPa, and $BaCe_{0.6}Zr_{0.4}O_3$ at 30 GPa. The spectra have been baseline corrected.

occurring in the group of $A_i$ bands as $x$ decreases (Fig. 1) may be related to the proportion of Ce–O and Zr–O stretching oscillators. As pressure increases and up to about 30 GPa, the evolution of mode wavenumbers is a continuous increase corresponding to a general increase of force constants. On the other hand, the evolution of the Raman spectra of the compounds $x = 0.6$ and $x = 0.8$ (Fig. 4) shows that these compounds undergo a phase transition, respectively, at 30 and 28 GPa. The $E_i$ and $B_i$ bands disappear above these pressures, and the new broad bands at 200, 500, and 800 $cm^{-1}$ characterize the apparition of a new phase. This evolution is similar to that of $BaCeO_3$, which undergoes a first-order transition at 22 GPa (Fig. 6) toward a structure with a lower symmetry (16) according to the increase of Raman band numbers. The Raman spectrum of this new phase is characterized by numerous bands between 400 and 600 $cm^{-1}$ and a narrow band near 200 $cm^{-1}$. Considering that pressure is not perfectly hydrostatic above 20 GPa, the broad band below 600 $cm^{-1}$ for $x = 0.8$ and $x = 0.6$ can be considered the envelope of the components observed in pure $BaCeO_3$ (Fig. 6) while the broad band at 800 $cm^{-1}$ is associated with the presence of Zr. Under this assumption, the structure of these high-pressure phases should be of low symmetry as for $BaCeO_3$. However, we cannot exclude that the bands' broadness, in addition to poorly resolved components, can also be due to a partial amorphization of the sample. This amorphization phenomenon has been observed on other perovskites (19). After the pressure release, spectra are similar to the initial ones for all compositions, which indicates the reversibility of the transitions.

In the pressure range [0–30 GPa], the apparition of thin bands (the whole spectrum in Fig. 2, $B_i$ band in Figs. 2–4) which increase in intensity, shows that the phase transition concerns the whole sample. Based on results obtained on pure $BaCeO_3$ (12, 13, 16), transitions toward phases of lower symmetry can be expected. The use of a high-pressure cell makes it difficult to investigate the Raman spectra below 100 $cm^{-1}$. Hence the number of observed $E_i$ bands in the 80–150 $cm^{-1}$ range cannot be used as an indicator of the structure as it is done in (8). We propose two other criteria to identify phase transitions:

(i) For $0.1 \leq x \leq 0.6$, the B band splits into two bands as pressure increases (Fig. 5). This splitting is also observed for $BaCeO_3$ with decreasing temperature. $BaCeO_3$ displays two bands ($B_1$ and $B_2$) at room temperature, and, when the $Imma \rightarrow R\bar{3}c$ transition takes place, the $B_1$ and $B_2$ bands merge into a single band B (13). Hence by comparison with $BaCeO_3$, we can assume that the splitting of the B band in mixed compounds indicates that the transition $R\bar{3}c \rightarrow Imma$ takes place as pressure increases. The $B_i$ bands involve Ba–O stretching and O–Ce–O bending, and their evolution is the indication that atoms progressively shift toward less symmetrical positions.

(ii) For $BaCeO_3$ in the *Pnma* structure, the $E_1$ and $E_2$ intensities decrease as temperature increases. Just after the transition $Pnma \rightarrow Imma$, the $E_1$ intensity increases at the expense of the $E_2$ intensity (13). These different evolutions are also observed in the mixed compounds spectra for $x = 0.8$ (Fig. 4) and $x = 0.6$ as pressure decreases. Assuming that $\Delta P < 0$ induces a $\Delta V > 0$ as for a temperature rise, these spectral changes can be used to determine approximately the pressure of the transition $Imma \rightarrow Pnma$. Genet *et al.* (17) note that even in $BaCeO_3$, this transition is not easy to observe in the Raman spectra.

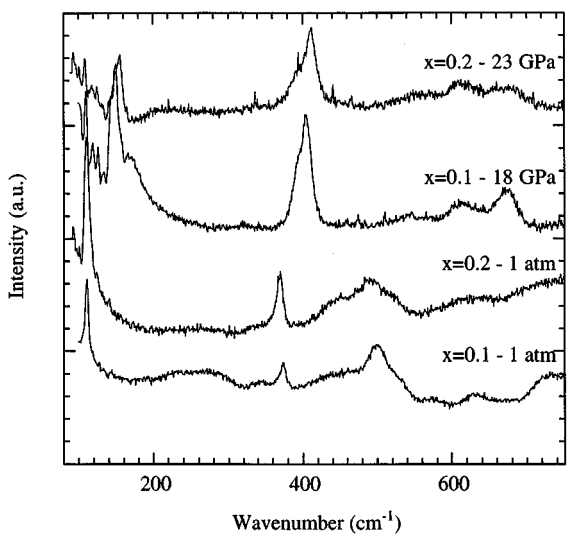


**FIG. 7.** Comparisons of the Raman spectra of $BaCe_{0.1}Zr_{0.9}O_3$ at 1 atm and 18 GPa, and, the Raman spectra of $BaCe_{0.2}Zr_{0.8}O_3$ at 1 atm and 23 GPa.

From these different criteria, we proposed a phase diagram of the mixed compounds $BaCe_xZr_{(1-x)}O_3$, $0 < x \le 1$, in Fig. 8. The major effect of Zr for Ce substitution is that it increases the transition-pressures. A neutron study (20) shows that, at room temperature and at room pressure, in the replacement of Zr for Ce, the size of the $BO_6$ octahedra decreases with $x$ at a higher rate than the lattice parameters. Therefore the driving force for the evolution toward a symmetric structure is increased, and it becomes more difficult to distort the perovskite structure.

### 4.2. From Nanophases to Homogeneous Solution

We are now going to show how the pressure effect on spectra can be interpreted as a continuous transition from model II, which describes the sample in terms of nanophases rich in Zr or in Ce, to model I, which corresponds to a fully random distribution of Ce and Zr on octahedral sites.

The $BaCe_{0.1}Zr_{0.9}O_3$ spectrum at 1 atm (Fig. 3) can be interpreted as the addition of 10% of the spectrum of $BaCeO_3$ in its $R\bar{3}c$ form (which indicates that these separate nanophases are interacting) and of 90% of the spectrum of $BaZrO_3$ (the intensity of which indicates that $BaZrO_3$ is not in an ideal $Pm3m$ structure). Under increasing pressure these separate spectral characteristics tend to disappear and to give rise to a common spectrum which could be a nearly perfect solution one. In the $BaCe_{0.2}Zr_{0.8}O_3$ spectrum at 1 atm (Fig. 7), the two narrow compounds characteristic of $BaCeO_3$ (B and E bands) are twice as intense as they are in the corresponding spectrum of the $x = 0.1$ compound; this confirms that the spectral components are independent at 1 atm and validates the nanophases' coexistence at low pressure as assumed in model II. However at high pressure the $x = 0.1$ and $x = 0.2$ spectra are similar (Fig. 7) to that of the pure $BaZrO_3$, with the exception of the $A_i$ bands at high frequencies, which are broadened in the solutions. In the same way, in the low-pressure range the $BaCe_{0.8}Zr_{0.2}O_3$ (Fig. 4) spectrum looks like that of $BaCeO_3$ in its *Imma* form while at high pressure (27 GPa) it looks similar to that of pure $BaZrO_3$ at high pressure (Fig. 2). Model II interprets the $R\bar{3}c$ form of $BaCeO_3$ nanophases in $BaCe_{0.1}Zr_{0.9}O_3$ in terms of a possible small interaction between $BaCeO_3$ and $BaZrO_3$ nanophases in order to explain the structural change from Pnma to $R\bar{3}c$. In $BaCe_{0.8}Zr_{0.2}O_3$, the $BaCeO_3$ nanophases are less distorted because of the smaller proportion of Zr. Under high pressure, the nanophases tend to disappear, to "melt" into homogeneous phase, the frontier atoms between nanophases being forced to be completely connected. Thus the low wavenumbers in the high-pressure spectrum, which correspond mainly to the O and Ba network vibrations (B and E bands), remain narrow in the solid solutions. For these modes Ce and Zr can be viewed as a mean atom M. On the other hand, high wavenumbers ($A_i$ bands) are broadened in the solid solutions compared to pure $BaZrO_3$ because these modes involve Zr–O and Ce–O bond stretching and reflect the short-range disorder. Recall that high wavenumber modes are characterized by a short correlation length compared to the low wavenumber modes (21). The same interpretation can be applied to $BaZrO_3$. In this latter case, the Raman spectrum loss from 1 atm to 9 GPa (Fig. 2) can be interpreted as the disappearance of nanodomains of lower symmetry than $Pm3m$, these nanodomains giving rise to first-order broad spectra at low pressure. As pressure increases the nanodomains interact and lead to a homogeneous phase with $Pm3m$ long-range order. Thus at high pressure, model I seems to be convenient for interpreting spectra. Notice that the bandwidths of high wavenumber modes in the solutions reveal that at short range the "mean atom" notion is lost and that the Ce and Zr distribution is responsible for their broadness. Finally, we would like to underline the reversibility of the spectra evolution for pure $BaZrO_3$ as well as for the other members. This reversibility proves that nanodomains (or nanophases) are not the result of incomplete reaction during sample preparation but correspond to a stable state of the sample at 1 atm and do not evolve to microdomains (or microphases) spontaneously even upon heating or upon high pressure.

### 4.3. Compressibility Properties of $BaCe_xZr_{(1-x)}O_3$ ($0 < x \le 1$)

*4.3.1. Definitions and model.* This second part is devoted to the derivation of sample compressibilities in order to search for a geometric criterion able to predict structural instability and phase transitions. These transitions depend on composition $x$, temperature $T$, or pressure $P$. Any shift of these parameters induces volume changes and therefore frequency shift. The method presented here, which is based on the Grüneisen model, has been developed by Hazen and Finger (22). The Grüneisen parameter correlates the pressure dependence of Raman mode frequencies with the unit cell volume and is defined by

$$\gamma_T = -\left(\frac{\partial \ln \nu}{\partial \ln V}\right)_T = \frac{1}{\chi}\left(\frac{\partial \ln \nu}{\partial P}\right)_T, \qquad [1]$$

where $\nu$ is the frequency of a vibrational mode, $V$ is the corresponding unit cell volume, and $\chi$ is the bulk compressibility given by

$$\chi = -\left(\frac{\partial \ln V}{\partial P}\right)_T = -\frac{1}{V}\left(\frac{\partial V}{\partial P}\right)_T, \qquad [2]$$

The method proposed here consists of remarking that the polyhedron symmetrical stretching mode involves mainly one type of force constant (17) and that the compressibility

of the polyhedron is determined by these microscopic force constants. Note that for structures in which the polyhedra are strongly distorted, this model fails because pure symmetrical stretching modes cannot exist anymore. Provided it is possible to identify such specific modes involving a single type of force constant, one can determine the individual compressibilities of octahedra, $\chi_o$, and dodecahedra, $\chi_d$. Assuming that the structures of the mixed perovskites studied in this paper are nearly cubic, the total compressibility, $\chi_{total}$, for the different compositions $x$, can be deduced from

$$\chi_{total} = \chi_o \frac{V_o}{V} + \chi_d \frac{V_d}{V}, \qquad [3]$$

where

$$\chi_o = x \cdot \chi_{CeO_6} + (1 - x) \cdot \chi_{ZrO_6} . \qquad [4]$$

Octahedra compressibilities $\chi_{CeO_6}$ and $\chi_{ZrO_6}$ can be obtained following the method given in (16). Assuming that $V$ varies linearly with $P$ in the low-pressure range ($< 10$ GPa) and that the compounds are nearly cubic, Eq. [2] becomes

$$\chi = -3 \frac{\Delta a}{a} \frac{1}{\Delta P}, \qquad [5]$$

where $a$ is the lattice parameter. Changes in $a$ and thus in bond distances $d$ induce changes in force constants $k$ and thus in vibrational frequencies $v$. This is the so-called quasi-harmonic approximation which assumes that $P$ (and $T$) affects the frequencies only through a volume variation. Different relationships between force constants $k$ and bond lengths $d$ have been proposed for ionic materials (13, 15). Assuming that force constants vary as $d^{-n}$ where $n$ is a parameter and introducing the harmonic oscillator relationship, one obtains

$$\chi = \frac{6}{n} \frac{\Delta v}{v} \frac{1}{\Delta P}. \qquad [6]$$

Thus the dodecahedra and octahedra compressibilities can be deduced from the slope of the linear sections of the curve $\omega = f(P)$ corresponding to a specific mode which involves a single type of force constant. The total compressibility is obtained from Eqs. [3] and [4]. Actually, if this model is believed to be reasonable for an octahedron, it is certainly much less adapted to dodecahedra for which the low-frequency $E_i$ modes are not pure stretching Ba–O modes as mentioned above. Moreover, the fact that Ce–O–Ce angles are far from 180° in the *Pnma* structure due to octahedra tilting must give rise to the conclusion that the actual compressibility of dodecahedra is higher than that obtained with the above method.

In an other way, diffraction studies (8, 14) show that structural transitions occur in the order *Pnma–Imma–*$R\bar{3}c$*–Pm3m* when temperature is raised or when Ce is replaced by Zr. From neutron diffraction study (20), the ratio, $r_v$, of the formula unit volume to the $BO_6$ octahedron volume has been shown to be a good indicator of the structure evolution of the solid solution versus temperature. For $r_v$ below 5.76, the structure is *Pnma*. It is *Imma* for $5.76 < r_v < 5.80$, $R\bar{3}c$ for $5.80 < r_v < 6$, and *Pm3m* for $r_v = 6$. It is possible to estimate this ratio versus pressure using compressibilities. By integrating Eq. [2] for the total compressibility, $\chi_{tot}$, and for the octahedra compressibility, $\chi_o$, we obtain

$$\frac{V_{tot}}{V_o} = \left(\frac{V_{tot}}{V_o}\right)_i . \exp[(\chi_o - \chi_{tot})P]$$
$$r_v = r_{vi} . \exp[(\chi_o - \chi_{tot})P], \qquad [7]$$

where $V_{tot}$ and $V_o$ are the total and octahedra volumes respectively and $r_i$ corresponds to the volumes ratio at ambient pressure, $r_{vi} = (V_{tot}/V_o)_{1atm}$.

Hence from the determination of compressibilities and from the use of a geometrical indicator, it is possible to estimate the phase transitions in the mixed perovskites $BaCe_xZr_{(1-x)}O_3$.

*4.3.2. Polyhedra compressibility and phase transitions.* As mentioned earlier, $E_i$ bands are mostly due to Ba–O stretching and O–Ba–O bending force constants, the A band is almost exclusively correlated to Ce–O stretching force constants, and the $B_i$ bands involve both Ba–O stretching and O–Ce–O bending. Hence the model proposed in 4.2.1. is applied to $A_i$ and $E_i$ bands involving mainly stretching $CeO_6$ octahedra and $BaO_{12}$ dodecahedra, respectively. $A_i$ bands display a two-mode behavior (8). The two-mode behavior is characterized by the simultaneous presence of the two end-member bands in the mixed crystals, sometimes associated with "local" modes ranging between them. In $Si_{(1-x)}Ge_x$ these bands have been attributed to Si–Si, Si–Ge, and Ge–Ge modes (7). In our case, $A_1$ and $A_3$ can be attributed, respectively, to vibrational modes involving $CeO_6$ octahedra and $ZrO_6$ octahedra. Hence Table 1 reports $\chi_{CeO_6}$, $\chi_{ZrO_6}$, and $\chi_{BaO_{12}}$ calculated from Eq. [6] applied to, respectively, $A_1$, $A_3$, and $E_i$ ($i = 1, 2$) between 0 and 10 GPa. It has been proposed (23) that force constants obey a law such as $k = d^{-n}$ with $n = 13$ for ionic compounds. This value allows us to obtain reasonable values for compressibilities of $BaCeO_3$ (13) and $SrCeO_3$ (24). Because of their chemical and structural similarity, it is reasonable in a first stage to transfer this value to $BaCe_xZr_{1-x}O_3$. Application of Eqs [3] and [4] allows us to calculate the total compressibility of each solid solution (Table 1, Fig. 9), using the values obtained from neutron

**TABLE 1**
**Compressibilities of Polyhedra Deduced from Wavenumbers of Stretching Modes (bands $A_1$, $A_3$ and $E_i$)**

| $x$ | 0 | 0.1 | 0.2 | 0.4 | 0.6 | 0.8 | 1 |
|---|---|---|---|---|---|---|---|
| $\chi_{CeO_6}$ | — | 0.80 | 0.62 | 0.71 | 0.77 | 0.81 | 0.95 |
| $\chi_{ZrO_6}$ | ? | 0.63 | 0.67 | 0.61 | 0.71 | 0.74 | — |
| $\chi_{BaO_{12}}$ | ? | 0.91 | 0.87 | 0.85 | 0.81 | 0.74 | 0.96 |
| $r_i$ | 6 | (5.99) | (5.97) | 5.91 | (5.85) | 5.79 | 5.67 |
| $\chi_{total}$ | ? | 0.87 | 0.83 | 0.81 | 0.80 | 0.75 | 0.96 |

*Note.* The ratio $r_i = (V_{tot}/V_o)_i$ at ambient pressure used in the calculation of the total compressibility is reported.

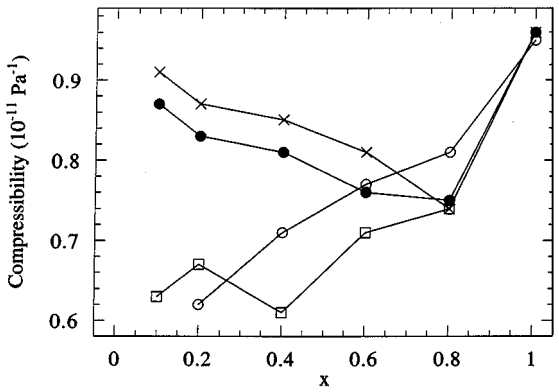


**FIG. 9.** Compressibilities of polyhedra (○, $CeO_6$; □, $ZrO_6$; ×, $BaO_{12}$) and total compressibility (●) of $BaCe_xZr_{1-x}O_3$ deduced from wavenumbers of $A_i$ and $E_i$ bands as a function of $x$.

diffraction for $V_o/V$ and $V_d/V$ at ambient pressure (20). Compressibility values are found in the range $[0.7 \times 10^{-11}$–$1.0 \times 10^{-11}\,Pa^{-1}]$ and close to $0.66 \times 10^{-11}$ $Pa^{-1}$ determined from macroscopic measurements of the bulk modulus and of the Poisson coefficient for $BaZrO_3$ (25). Octahedra compressibilities $\chi_{CeO_6}$ and $\chi_{ZrO_6}$ are found to increase from $BaZrO_3$ to $BaCeO_3$ (Fig. 9) due to the frequency dependence of compressibilities (Eq. [6]). The same trend was obtained from combined diffraction results and Raman scattering (26). Table 2 reports the average $B$–O ($B$ = Ce, Zr) distance in the mixed perovskites measured by neutron diffraction (14, 20). The $d(B$–O) increases from $BaZrO_3$ to $BaCeO_3$, hence we can expect that the compressibility of the octahedra increases from $BaZrO_3$ to $BaCeO_3$ as is observed in Fig. 9. What is more unexpected is the fact that $\chi_{CeO_6}$ and $\chi_{ZrO_6}$ are found close to each other for any $x$ value. The total compressibility ($\chi_{total}$) decreases from $x = 0.1$ to $x = 0.8$, this trend being imposed by the compressibility of dodecahedra (Eq. [3]), which decreases in this $x$ range. Because $\chi(BaZrO_3)$ $(0.66 \times 10^{-11}\,Pa^{-1})$ is lower than $\chi(BaCeO_3)$ $(0.96 \times 10^{-11}\,Pa^{-1})$, the inverse behavior was expected. Conversely, $\chi_{total}$ is found to increase from $x = 0.8$ to pure $BaCeO_3$.

The behavior of the ratio, $r_v$, of the formula unit volume to the octahedron volume with pressure can be determined from Eq. [7] (Fig. 10) and a phase diagram can be obtained using the critical values of $r_v$, 5.76, 5.80, and 6.00 (Fig. 11). The pressure-induced transitions are expected in the range of pressures investigated in this study. The calculated domain of existence of the structure $R\bar{3}c$ is reasonable compared to the experimental domain while the calculated *Imma* domain is overestimated. These results show that if structural changes can be predicted from polyhedra compressibilities, it is difficult to rely on calculated pressures. Comparison between Fig. 8 and Fig. 9 allows us to appreciate the discrepancies between the experimentally based and the calculated phase diagrams. This poor agreement can have several origins: (i) noticing that $\chi_{total}$ is mostly determined by $\chi_{BaO_{12}}$ and that this term can be overestimated, as already said, the calculated compressibilities do not correspond to the actual compressibilities and the behavior of the

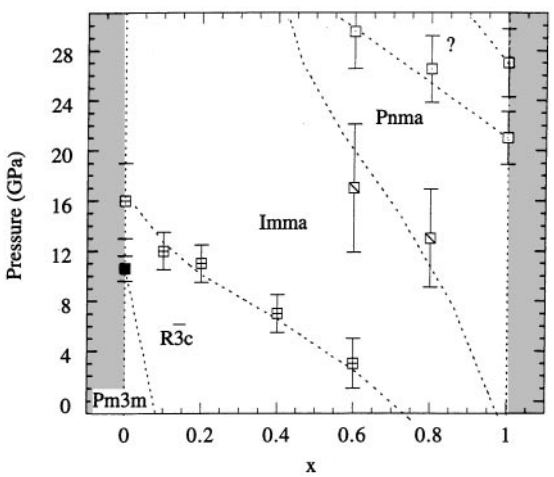


**FIG. 8.** Phase diagram of $BaCe_xZr_{1-x}O_3$ established from Raman spectra.

**TABLE 2**
**Average $B$–O ($B$ = Ce, Zr) and Ba–O Distances from Neutron Diffraction Data (12) for Various Compositions in the $BaCe_xZr_{1-x}O_3$ System at Room Temperature and Room Pressure**

| $x$ | 0 ($Pm3m$) | 0.1 ($Pm3m$) | 0.4 ($R\bar{3}c$) | 0.8 ($Imma$) | 1 ($Pnma$) |
|---|---|---|---|---|---|
| $\bar{d}_{B-O}$ (Å) | 2.099 | 2.1087 | 2.1511 | 2.2038 | 2.2392 |
| $\sigma_{B-O}$ | 0 | 0 | $5 \times 10^{-5}$ | $3.4 \times 10^{-3}$ | $1.25 \times 10^{-2}$ |
| $\bar{d}_{Ba-O}$ (Å) | 2.968 | 2.982 | 3.039 | 3.089 | 3.125 |
| $\sigma_{Ba-O}$ | 0 | 0 | 0.158 | 0.249 | 0.336 |

*Note.* Standard deviations $\sigma = \sqrt{(\sum_i d_i^2 - n \cdot \bar{d}^2)/n - 1}$ (with $n$ as the number of data points and $\bar{d}$ as the mean of the data) are also reported.

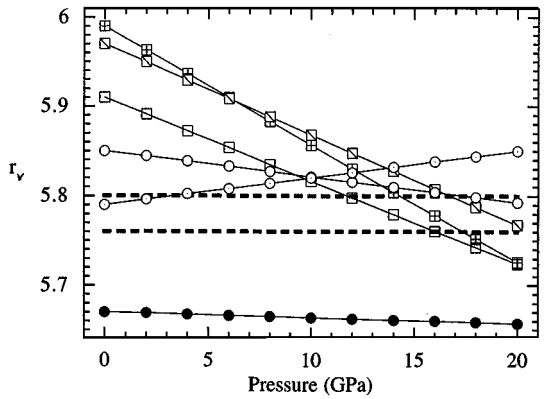


**FIG. 10.** $r_v = f(P)$ plots for each solid solution: $x = 0.1$(■), $x = 0.2$ (⧅), $x = 0.4$ (□), $x = 0.6$ (○), $x = 0.8$ (⊙), and $x = 1$ (●). Critical values of $r_v$, 5.76 and 5.80, are represented by the dotted lines.

$V_{tot}/V_o$ ratios with pressure, from which the transition pressures are deduced, is altered; (ii) in an other way, the phenomenological criterion, $r_v$, is chosen according to thermal experiments (20) as mentioned in 4.3.1. Other criteria could be considered, such as A–O and B–O average distances. High-pressure studies by X-ray diffraction are in progress and will help to confirm whether the $r_v$ criterion is valid with respect to pressure or whether other criteria such as the standard deviation could be pertinent.

## 5. CONCLUSION

These results allow us to reach two of the objectives which stimulated this study. $BaZrO_3$ can be viewed at 1 atm as made of nanodomains without long-range ordering. As pressure increases (up to 9 GPa) these nanodomains are forced to interact more strongly and lead to a continuous structure with long-range order. In the high-pressure range, structural changes on a long range order scale are observed. Solid solutions at 1 atm can also be described in terms of nanophases rich in Zr or in Ce. As pressure increases, these nanophases tend to disappear and lead to a homogeneous phase.

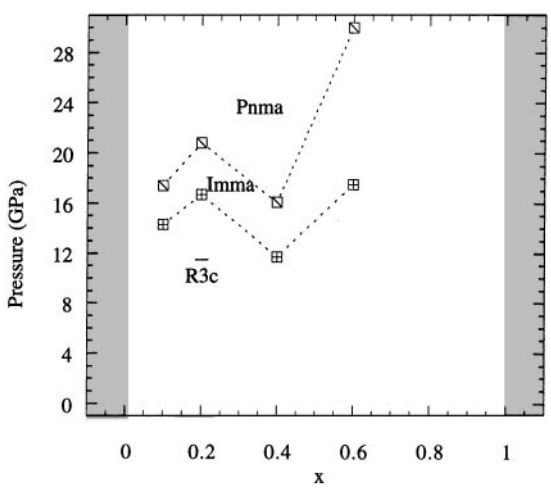


**FIG. 11.** Phase diagram of $BaCe_xZr_{1-x}O_3$ established from Fig. 8.

The high-pressure Raman study of $BaCe_xZr_{1-x}O_3$ up to 30 GPa allows us to identify several phase transitions. Compressibilities are derived from $P$ dependencies of modes involving specifically individual polyhedra of the structure. Calculated compressibilities of octahedra are found to be in good agreement with other studies (25). Using the ratio of the formula unit volume to the $BO_6$ octahedron volume as a phenomenological criterion, a tentative phase diagram is proposed. This method is adapted to materials for which Raman spectra present specific stretching modes corresponding to each polyhedra. The discrepancies between the calculated phase diagram and experimental data can be attributed to the difficulty in obtaining the dodecahedra compressibility from Raman spectra and to the choice of a geometrical criterion for phase transitions. A high-pressure study by X-ray diffraction of some of these mixed compounds is in progress.

## ACKNOWLEDGMENTS

We are grateful to Y. Lombart and D. Machon for their contributions to experiments and discussions.

## REFERENCES

1. A. R. West, "Solid State Chemistry and its Applications," p. 358. Wiley, Great Britain, 1984.
2. J. Chen, H. M. Chan, and M. P. Harmer, *J. Am. Ceram. Soc.* **72**(4), 593 (1989).
3. C. Boulesteix, F. Varnier, A. Llebaria, and E. Husson, *J. Solid State Chem.* **108,** 141 (1994).
4. E. Husson, L. Abello, and A. Morell, *Mater. Res. Bull.* **25,** 539 (1990).
5. W. B. White, "The Infrared Spectra of Minerals" (V. C. Farmer, Ed.), Vol. 6, p. 87. Mineralogical Society, London, 1974.
6. R. K. Chang, B. Lacina, and P. S. Pershan, *Phys. Rev. Lett.* **17,** 755 (1966).
7. M. I. Alonso and K. Winer, *Phys. Rev. B* **39,** 10056 (1989).
8. I. Charrier-Cougoulic, T. Pagnier, and G. Lucazeau, *J. Solid State Chem.* **142,** 220–227 (1999).
9. T. Scherban, W.-K. Lee, and A. S. Nowick, *Solid State Ionics* **28–30,** 585 (1988).
10. H. Iwahara, T. Yajima, T. Hibino, K. Ozaki, and H. Suzuki, *Solid State Ionics* **61,** 65 (1993).
11. I. Cougoulic-Charrier, Thesis, INPG Grenoble, 1998.
12. K. S. Knight, *Solid State Ionics* **74,** 109 (1994).
13. S. Loridant, Thesis, INPG Grenoble, 1997.
14. I. Charrier Cougoulic, T. Pagnier, G. Lucazeau, and C. Ritter, "ILL Experimental Report 5-23-474," Instrument D2B, www.ill.fr, 1998.

15. R. M. Hazen, "Microscopic to Macroscopic, Atomic environments to Mineral Thermodynamics, Reviews in Mineralogy" (S. W. Kieffer and Navrotsky, Eds.), Vol. 14, p. 317. 1985.
16. S. Loridant and G. Lucazeau, *J. Raman Spectros.* **30,** 485 (1999).
17. F. Genet, S. Loridant, and G. Lucazeau, *J. Raman Spectrosc.* **28,** 283 (1997).
18. G. J. Piermarini, S. Block, J. D. Barnettand, and R. A. Forman, *J. Appl. Phys.* **46,** 2774 (1975).
19. P. Gillet, *Phase Transitions* **63**(1–4), 77 (1997).
20. T. Pagnier, I. Charrier-Cougoulic, C. Ritter, and G. Lucazeau, *J. Europ. Physics* (in press).
21. E. K. H. Salje, *Phase Transitions* **37,** 83 (1992).
22. R. M. Hazen and L. W. Finger, *J. Geophys. Res.* **84,** 6723 (1979).
23. W. F. Sherman and G. R. Wilkinson, *in* "Advances in Infrared and Raman Spectroscopy" (R. J. H. Clark and R. E. Hester, Eds.), Vol. 6, p. 232. Hayden, New York, 1983.
24. G. Lucazeau, T. LeBihan, L. Abello, S. Loridant, and H. Libotte, to be published.
25. G. Goretta, E. T. Park, R. E. Koritala, M. M. Cuber, E. A. Pascual, Nan Chen, A. R. de Arellano-Lòpez, and J. L. Routbort, *Physica C* **309,** 245–250 (1998).
26. T. Pagnier, C. Chemarin, and G. Lucazeau, to be submitted.